The First Example of a μ 2 -Imido Functionality Bound to a Lanthanide Metal Center: X-ray Crystal Structure and DFT Study of [(μ-ArN)Sm(μ-NHAr)(μ-Me)AlMe2]2 (Ar = 2,6-iPr2C6H3)

John Gordon, Garth Giesbrecht, David Clark, P. Jeffrey Hay, D. Webster Keogh, Rinaldo Poli, Brian Scott, John Watkin

The First Example of a μ_2-Imido Functionality Bound to a Lanthanide Metal Center: The X-Ray Crystal Structure and a DFT Study of $[(\mu\text{-ArN})Sm(\mu\text{-NHAr})(\mu\text{-Me})AlMe_2]_2$ (Ar = 2,6-*i*-$Pr_2C_6H_3$)

John C. Gordon,*[1a] Garth R. Giesbrecht,[1b] David L. Clark,[1c] P. Jeffrey Hay,[1d] D. Webster Keogh,[1e] Rinaldo Poli,[2] Brian L. Scott,[1a] and John G. Watkin[1a]

Chemistry (C) Division, Nuclear Materials Technology (NMT) Division, Theoretical (T) Division and the Glenn T. Seaborg Institute for Transactinium Science, Los Alamos National Laboratory, Los Alamos, NM 87545

and

Laboratoire de Synthèse et d'Electrosynthèse Organomètalliques (LSEO UMR 5632), Universitè de Bourgogne, Facultè de Sciences "Gabriel", 6 boulevard Gabriel, 21000 Dijon, France

Abstract

Reaction of three equivalents of 2,6-di-*iso*-propylaniline with $Sm[N(SiMe_3)_2]_3$ affords the dimeric species $[Sm(NHAr)_3]_2$ (**1**). X-ray crystallography illustrates that each metal center in **1** engages in an η^6-arene interaction with the aryl ring of an amide ligand attached to an adjacent samarium. IR spectroscopy indicates that the π-arene interactions are maintained in solution. Reaction of **1** with four equivalents of trimethylaluminum leads to formation of the bis-μ_2-imido complex $[(\mu\text{-ArN})Sm(\mu\text{-NHAr})(\mu\text{-Me})AlMe_2]_2$ (**2**). The molecular structure of **2** contains a unique central Sm_2N_2 core which displays extremely short bridging Sm-N distances of 2.152(8) and 2.271(7) Å, characteristic of an imido complex. Density Functional Theory (DFT) calculations have been carried out in order to gain a better understanding of the nature of the bonding interactions within complex **2** and indicate that the 5d metal acceptor orbitals play a significant role in stabilizing π-donation from the imido groups to the samarium centers within the Sm_2N_2 core.

Introduction

The chemistry of metal-nitrogen multiply-bonded complexes has witnessed a dramatic surge in interest in recent years[3-9] due to the ability of the M=N functionality to undergo a wide range of reactivity, including metathesis of imines, aldehydes and carbodiimides, metallacycle formation with alkenes and alkynes, dealkylation and C-H bond activation.[10-17] Imido-containing complexes have been documented for the majority of the transition metals, and also the actinides.[18-25] Notable by their absence, however, are examples of terminal imido complexes of scandium, yttrium or the lanthanide elements. There have been two previous reports of structurally-characterized complexes which contain imido ligands bridging multiple lanthanide metal centers: (i) two μ_3-phenylimido ligands cap the tetranuclear core of the complex $[Yb_4(\mu\text{-}\eta^2\text{:}\eta^2\text{-}Ph_2N_2)_4(\mu_3\text{-}NPh)_2(THF)_4]$,[26] and (ii) a μ_4-NH ligand lies at the center of the tetranuclear complex $[\{(\eta^5\text{-}\mu_2\text{-}C_9H_6SiMe_2NH)Ln\}_2(\mu_3\text{-}Cl)(THF)]_2(\mu_4\text{-}NH)(THF)$.[27] Following a report by Evans *et al.* that trialkylaluminum reagents were capable of deprotonating anilido ligands,[28] we chose to examine whether the use of a sterically encumbered anilido ligand on a lanthanide metal center would allow the trialkylaluminum-mediated formation of an imido functionality. As a result, we describe here the isolation and characterization of a dimeric samarium amido-imido compound which provides clear structural insight into the behavior of an imido functionality on a lanthanide metal center.[29]

Results and Discussion

Reaction of $Sm[N(SiMe_3)_2]_3$[30] with three equivalents of 2,6-di-*iso*-propylaniline in toluene produces the brick-red complex $[Sm(NHAr)_3]_2$ (**1**) (Ar = 2,6-*i*-$Pr_2C_6H_3$) in moderate yield (eq. 1). Compound **1** is only sparingly soluble in toluene or hexane. The poor solubility of

1 in nonpolar solvents and its high reactivity towards donor solvents, coupled with the paramagnetism of Sm(III), did not facilitate characterization by NMR spectroscopy.

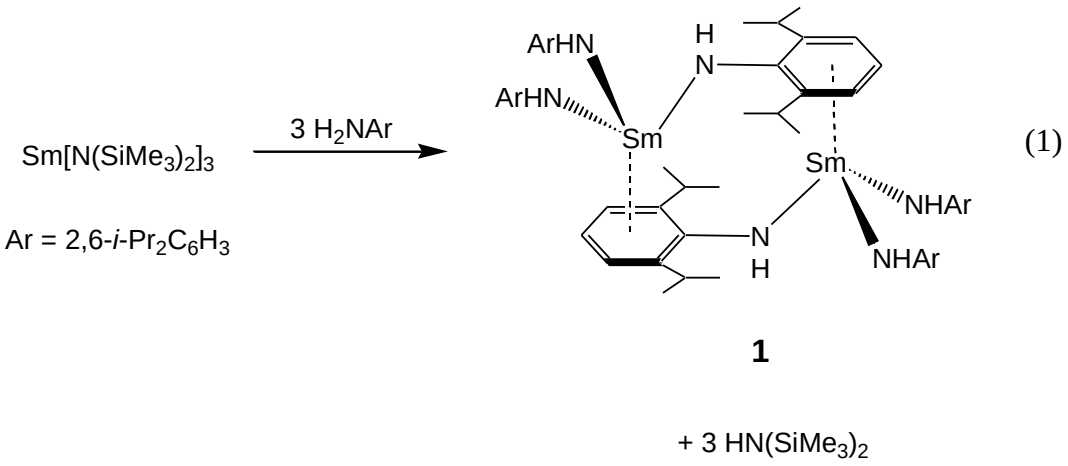

(1)

Slow evaporation of a saturated hexane solution of **1** yielded orange plates that were suitable for X-ray diffraction. The molecular structure of compound **1** is presented in Figure 1. A list of relevant bond lengths and angles is available in Table 1; complete details of the structural analyses of compounds **1** and **2** are listed in Table 3. Complex **1** possesses a π-arene-bridged dimeric structure analogous to that reported for the yttrium analog; however, in that case, the X-ray crystal structure was not of sufficient quality to allow for a detailed discussion of bond lengths and angles.[29] In the solid state structure of **1**, each samarium atom is ligated by three nitrogen atoms. Additionally, each metal center engages in an η^6-arene interaction with the aryl ring of an amide ligand attached to an adjacent samarium. The three nitrogen atoms and the aryl ring centroid support a tetrahedral geometry around the metal atom, with the angles anchored by the samarium atom ranging from 92.6(3)° to 117.6°. The distances between the metal center and the six carbon atoms of the aryl ring range from 2.838(10) to 3.094(10) Å with an average distance of 2.952(10) Å (Sm(1)-arene(cent) = 2.596 Å). This average Ln-C bond distance is

similar to those reported for the related aryloxide species $[Sm(O\text{-}2,6\text{-}i\text{-}Pr_2C_6H_3)_3]_2$[31] (2.986(8) and 3.016(8) Å for the two independent molecules in the asymmetric unit) as well as other known examples of compounds containing trivalent 4f element-π-arene interactions (*e.g.* average Ln-C distances of 2.89(3) and 2.91(6) Å have been reported for $(\eta^6\text{-}C_6Me_6)Sm(AlCl_4)_3$[32] and $(\eta^6\text{-}C_6H_6)Sm(AlCl_4)_3$,[33] respectively, while the intramolecular π-arene interaction in $Yb(O\text{-}2,6\text{-}Ph_2\text{-}C_6H_3)_3$ exhibits an average Ln-C distance of 2.978(6) Å.[34]). The Ln-C distances determined for compound **1** are significantly longer than the Gd-C(ave) distance of 2.630(4) Å found for the zerovalent complex, $Gd(\eta^6\text{-}t\text{-}Bu_3C_6H_3)_2$[35] and are slightly longer than the distances found in $\{[PhP(CH_2SiMe_2NSiMe_2CH_2)_2PPh]Ln\}_2\{\eta^6\text{:}\eta^6\text{-}(C_6H_5)_2\}$ (Ln = Y,[36] Ho[37]), in which the lanthanide centers interact with the phenyl rings of a dianionic bridging biphenyl unit. The bonds between samarium and the two nitrogens of the terminal amido ligands in **1** (2.241(8) and 2.273(11) Å) are slightly shorter than the $Sm\text{-}N_{bridging}$ distance (2.351(10) Å) and are unremarkable for samarium-amido bonds.[38]

The infrared spectrum of $[Sm(NHAr)_3]_2$ (KBr plates, Nujol) exhibits two distinct ν(C=C) stretching modes in the aromatic region (1590 and 1575 cm^{-1}), consistent with two different arene environments in the solid state. Similar features have been observed in the solid state and solution infrared spectra of $[Sm(O\text{-}2,6\text{-}i\text{-}Pr_2C_6H_3)_3]_2$ (1586 and 1572 cm^{-1}).[31] The solution IR spectrum of **1** (benzene solution) also displays two ν(C=C) stretching modes in the aromatic region (1590 and 1572 cm^{-1}), suggestive of the fact that the solid state η^6-bridged arene structure is maintained in solution. Although a dimeric structure involving anilido ligands bridging through nitrogen is also possible, the ν(C=C) stretching frequencies in this case might be expected to be so similar that they would not be resolved as two distinct bands.[39,40]

Treatment of **1** with four equivalents of trimethylaluminum in toluene, followed by crystallization from hexane, leads to isolation of the trialkylaluminum adduct [(μ-ArN)Sm(μ-NHAr)(μ-Me)$AlMe_2$]$_2$ (**2**) in moderate yield (eq. 2).

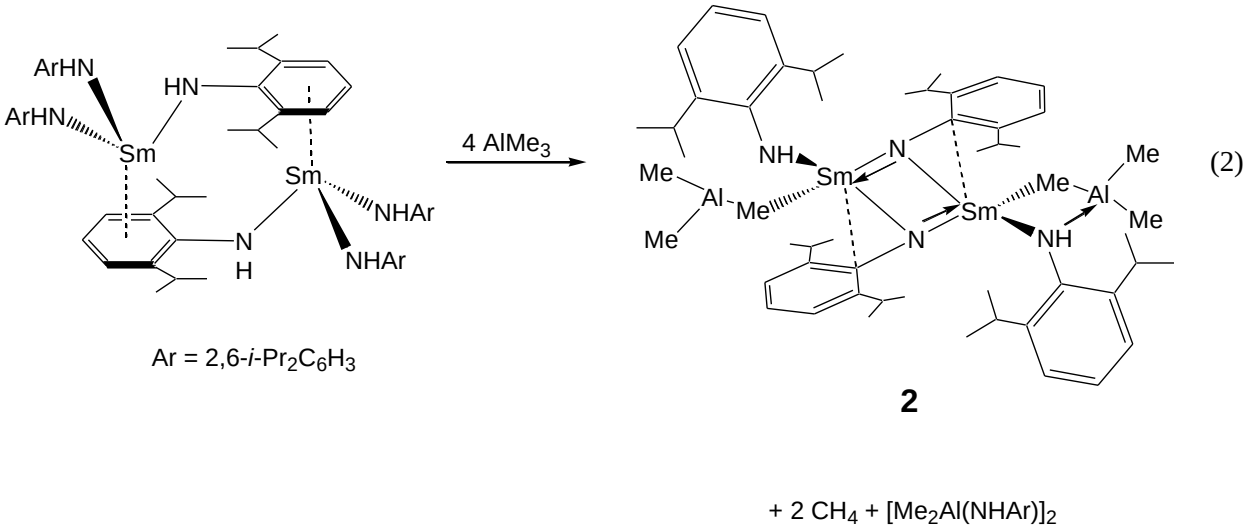

(2)

Compound **2** is extremely soluble in hydrocarbon solvents such as hexane and hexamethyldisiloxane. However, the similar solubility of the aluminum-containing byproduct [$Me_2Al(NHAr)]_2$ hampers the isolation of **2** in pure form. Multiple recrystallizations from hexane failed to separate complex **2** from the aluminum dimer. ^{1}H NMR spectroscopy revealed a series of sharp resonances assignable to the aluminum dimer and several broad, unassignable resonances, presumably due to complex **2**. Attempts to purify **2** by extraction into hexamethyldisiloxane resulted in a deep red solution and a colorless precipitate of [$Me_2Al(NHAr)]_2$, which was removed by filtration. Removal of the solvent and re-examination by NMR spectroscopy still revealed the presence of the aluminum complex. Multiple iterations of the extraction/filtration procedure proved unsuccessful in the isolation of pure **2**. At this point, we suspected that the residual aluminum complex was being generated in solution as a

result of the decomposition of **2**. We have recently observed similar redistribution reactions in related 4f-element complexes supported by phenoxide ligation.[41] However, thermolysis experiments did not indicate any significant decomposition, suggesting that difficulties in obtaining pure samples of **2** are due to the similar solubility properties of $[Me_2Al(NHAr)]_2$ and $[(\mu\text{-ArN})Sm(\mu\text{-NHAr})(\mu\text{-Me})AlMe_2]_2$ (**2**).[42]

Red crystals of **2** that were suitable for an X-ray structure determination were obtained from hexane. An ORTEP representation of compound **2** is available in Figure 2; selected bond lengths and angles are presented in Table 2. The X-ray diffraction study of **2** revealed a dimeric samarium amido-imido complex, lying on a crystallographic inversion center, in which the two samarium metal centers are asymmetrically bridged by two μ_2-imido ligands. Each metal center also bears a terminal -NHAr ligand, the nitrogen lone pair of which is coordinated to a trimethylaluminum molecule. Sm-N bond lengths within the central Sm_2N_2 core are unusually short, as expected for bridging imido (NR^{2-}) as opposed to bridging amido (NR_2^-) linkages. The two unique Sm-N distances within the Sm_2N_2 core are 2.152(8) and 2.271(7) Å. In comparison, typical Sm-N distances for bridging amido ligands are much longer, as exemplified by the distances of 2.468(7) and 2.614(7) Å in $[K(THF)_6]_2[Sm(\mu\text{-NHAr})(NHAr)_3]_2$ (Ar = 2,6-$Me_2C_6H_3$).[29] In fact, the bridging Sm-N distances in **2** are comparable to, if not shorter than, those found for typical terminal samarium amido ligands, for example 2.284(7) Å in $Sm[N(SiMe_3)_2]_3$,[43] 2.331(3) Å in $(\eta^5\text{-}C_5Me_5)_2Sm(NHPh)(THF)$,[44] and 2.218(5) and 2.202(5) Å in $\{(i\text{-}Pr_2N)_2SmCl_3[Li(TMEDA)]_2\}$.[38]

The asymmetry of the Sm_2N_2 core is further compounded by the presence of a significant interaction between the *ipso* carbon of the bridging μ-NAr ligand and one of the samarium metal centers (Sm(1)-C(1) = 2.666(8) Å). This results in an acute Sm(1)-N(1)-C(1) angle of 90.2(5)°,

and a correspondingly obtuse Sm(1*)-N(1)-C(1) angle of 168.1(8)°. The angles about each bridging nitrogen atom sum to 357.2°, indicating near-planarity of the substituents, and hence an almost perfect T-shape coordination geometry about nitrogen. Similar interactions with phenyl rings have been observed previously in bis(μ_2-imido) complexes of uranium[22,25,45,46] and zirconium.[20] In contrast to the very short Sm-N bridging distances, the terminal amido Sm(1)-N(2) distance is extremely long (2.535(8) Å), presumably as a result of the nitrogen-coordinated $AlMe_3$ molecule preventing π-donation of the lone pair to the metal center. We also note the structural similarity of **2** to the bismuth amido-imido complex $[Bi(NHAr)(\mu\text{-}NAr)]_2$,[47] although in the case of the bismuth complex no interaction with the bridging phenyl ring was observed.

Compound **2** also maintains a short Sm-C distance (*i.e.* aluminum bound methyl group) of 2.649(14) Å, which is similar to the Sm-C(alkyl group) distances previously determined for $(ArO)Sm[\mu\text{-}OAr)(\mu\text{-}R)AlR_2]_2$ (R = Me (2.620(5) and 2.632(5) Å);[48] Et (2.627(4) and 2.649(4) Å).[41] This distance is slightly shorter than typical Ln-C distances found in complexes containing bridging methyl groups[49-52] and suggests the presence of an agostic interaction between the aluminum methyl group(s) and the metal center. There is also a distinct elongation of the Al-C bond associated with the "agostic" methyl group (Al(1)-C(25) (2.094(12) Å) vs. Al(1)-C(26) (1.939(12) Å) and Al(1)-C(27) (1.971(11) Å)). DFT calculations, however, suggest that this interaction may be more accurately described as a bridging methyl group, based on electronic considerations (see later).

Theoretical Studies on Complex 2

Structural results using realistic ligands. Since, to the best of our knowledge, complex **2** represents the first structurally characterized example of a discrete imido complex of a 4f-

element, we were interested in obtaining a more detailed picture of the bonding interactions that stabilize the Sm_2N_2 core within this molecule. DFT calculations employing the B3LYP functional were carried out on the dimeric model species, $[(\mu\text{-PhN})Sm(\mu\text{-NHPh})(\mu\text{-Me})AlMe_2]_2$ species (Fig. 3), in which the isopropyl substituents on the bridging and terminal phenyl groups were replaced by hydrogen atoms. The structure was optimized using the basis sets and effective core potentials (ECPs) on Sm described in the Experimental Section. The partially occupied $4f^5$ shell was incorporated into the "large core" ECP, leaving the 5d and 6s orbitals as the most important valence orbitals. Recent studies on $Ln(NH_2)_3$ and $Ln[N(SiH_3)_2]_3$ (Ln = La through Lu) model complexes have shown that accurate results may be obtained without the inclusion of the f electrons in the valence shell.[53,54] We have also found that "large core" provide results comparable to those of calculations which explicitly included the $4f^5$ shell for larger complexes such as $Ln[CH(SiMe_3)_2]_3$.[55] These calculations also effectively describe the agostic interactions present in molecules such as the aforementioned $Ln[N(SiMe_3)_2]_3$[55] and $Sm[CH(SiMe_3)_2]_3$.[56]

Comparing some of the key geometrical parameters between the optimized structure and the experimental structure (Table 4) we see that the Sm-N bridging bond lengths are calculated to be 2.220 Å (Sm=N) and 2.299 Å (Sm-N) (differing by 0.08 Å), as compared to the experimental values of 2.153 Å (Sm=N) and 2.271 Å (Sm-N) (differing by 0.11 Å). Overall the calculations appear to be giving a reasonable description of the multiple bond character in the Sm-imido linkage. In addition, the calculated bond length of the longer Sm-N terminal bond (2.55 Å) agrees well with the observed bond length (2.535 Å).

The results of the calculations illuminate the nature of the Sm-(μ-CH_3)-Al interactions, since the accurate locations of the methyl hydrogen atoms are not available from the experimental X-ray structure. The coordination geometry at the bridging carbon atom can be

described as distorted trigonal bipyramidal, with the Sm atom and one H atom occupying axial positions, while the Al atom and the two remaining H atoms take up the equatorial positions (see Figure 3). The Al-CH_3 moiety is therefore arranged in a staggered conformation relative to the Al···Sm axis. In addition, relative to the Al-C axis, the methyl group is titled away from the Sm atom, as evidenced by the smaller than tetrahedral Al-C-H angle to the axial H atom and the larger ones to the two equatorial H atoms. Thus, the μ-CH_3 ligand is best described as a bridging methyl group, similar to the situation observed in Al_2Me_6, and not as an Al-CH_3 group establishing agostic interactions with the Sm atom. In other words, both C-Al and C-Sm interactions are established with the same carbon electrons.

To probe some of the factors affecting the multiple bonding of the imido fragments within the dimer, three additional sets of calculations were performed where each structure was re-optimized to compare to the original complex: (a) the $AlMe_3$ groups were removed entirely; (b) the original dimer was calculated without 5d basis functions on the Sm atoms and; (c) the full dimer was maintained but the Ph substituents on the bridging and terminal ligands were replaced by methyl groups. These results are also summarized in Table 4. Removing the Lewis acidic $AlMe_3$ groups has surprisingly little effect on the bond lengths in the bridging Sm_2N_2 unit, with the bond alternation actually modestly enhanced. The Sm-N terminal bond becomes 0.2 Å shorter when the nitrogen is no longer complexed to the aluminum center, as one would expect since more electron density is now available on the nitrogen for bonding to the samarium center in the absence of the Lewis acid. This result indicates that the trimethylaluminum groups do not directly affect the electronic structure of the Sm_2N_2 core, but rather have a steric function, with the –NH($AlMe_3$)Ph groups acting as bidentate, uninegative ligands.

In contrast, replacing the N-Ph groups with N-Me groups results in a nearly symmetric Sm-N-Sm linkage, with the two Sm-N bond lengths differing by less than 0.01 Å. The Sm-N_{br}-C angle (153° in the case of N-Ph) changes to 131° for the bridging N-Me group, suggesting that π-overlap with the phenyl ring plays an important part in maintaining the double-bond character in the Sm=N-Ph bridging bonds. These results are consistent with those reported by Andersen *et al*. for the uranium complexes, $(MeC_5H_4)_4U_2(\mu\text{-}NR)_2$ which exhibit symmetric (R = $SiMe_3$) or asymmetric (R = Ph) bridging imido groups depending on the nature of the organic constituent.[45] In that case, the asymmetry in the structure of $(MeC_5H_4)_4U_2(\mu\text{-}NPh)_2$ was ascribed largely to the contributions of an η^3-azabenzylic resonance structure in which negative charge was delocalized to the ortho and para positions of the phenyl ring, although the presence of C-N π-bonding was not conclusively established.

The net charge on the Sm centers from the population analysis in the most realistic model is +1.14, (*i.e*. much less ionic than the formal oxidation state of +3). There is considerable donation of electron density into the 5d orbitals as evidenced by the overall d population of 1.28 electrons. The remaining valence population of 0.56 electrons involves the 6s and 6p orbitals. The particular importance of d orbital participation is illustrated in the results of Table 4. In the absence of 5d functions on samarium, a lengthening of 0.09 and 0.11 Å in the calculated Sm=N and Sm-N bond distances is observed. This represents an overall increase in bond distances of approximately 7% relative to the metric data garnished by the X-ray study. These results show that in their role as π-acids, the 5d orbitals play an important role in the stabilization of the Sm=N fragment (see later). The population analysis also suggests that it is more accurate to view the bonds involving the samarium center as covalent bonds, in contrast to the commonly held view of bonds involving the lanthanides as being predominantly ionic in nature.

Bonding analysis and results from model calculations. In considering the bonding in the Sm dimers it is useful to consider the frontier MOs of the bridging $[N\text{-}Ph]^{2-}$ ligand (Scheme 1). The nitrogen atom can be thought to have three electron pairs: the σ lone pair (n_σ) and two p lone pairs, one conjugated with the π electrons of the phenyl group ($\pi_\perp$), and one parallel to the ring ($\pi_\parallel$). We would expect these MOs on each bridging nitrogen atom to play an important role in the Sm-N bonding. Indeed, we find the highest two occupied MOs correspond to the symmetric and anti-symmetric combinations of the N$p\pi_\perp$ orbitals interacting with the Sm centers. Contour plots of these orbitals are shown in Fig. 4 (designated as MOs 147 and 148). A bonding analysis of these MOs (Table 5) shows approximately 3 percent 5d orbital contribution from each Sm center for the HOMO (MO 148) and about 8 percent 5d contribution from each Sm center for the next highest MO (MO 147). Therefore, while the composition of these MO's are mainly ligand based in nature, the overall metal orbital contribution is essentially dominated by the 5d orbitals on each metal center (roughly 75% of the metal based contribution from Sm_a and Sm_b is 5d in nature in MO 148, while in MO 147 it is closer to 90%).

At slightly lower energies one finds the symmetric and antisymmetric combinations of the N$p\pi_\parallel$ ligand orbitals interacting with the Sm centers (MOs 143 and 146), which also have significant 5d orbital participation (6 and 7 percent, respectively). Together these four MOs account for 0.54 electrons of the 1.28 5d electrons from the population analysis. One finds orbitals involving the n_σ ligand combinations at much lower binding energies. Finally, some of the MOs involved in the bonding of the terminal NHPh groups to the Sm ions are also found, denoted as Sm-N_t p$\pi_\perp$orbitals in Table 5, at similar energies to the orbitals described above.

To probe the bonding interactions more clearly, calculations on simpler model systems were performed in which all amido and aluminum substituents (except for the methyl group

which bridges the aluminum and samarium atoms) were replaced with hydrogen atoms. The N-Ph bridging ligand was maintained. The optimized structure of this simplified model yielded similar geometrical parameters to the more realistic models (Table 4), and the structures are compared in Figure 5. The simpler model resulted in a lengthening of the Sm-$C_{\text{bridging methyl}}$ bond length from 2.71 Å to 2.87 Å and in a shortening of the Sm-N_t bond length from 2.55 Å to 2.44 Å, leading to a shift of the Al atoms to the opposite side of the $Sm_2(\mu\text{-}N)_2$ plane, as seen in Figure 5(b). The configuration adopted by the simpler model probably reflects the actual electronic preference of the molecule, since the four bonds to each samarium atom (namely the Sm-N_t, the Sm-CH_3, and the two Sm-N_b bonds) are closer to the ideal tetrahedral configuration. The distortion observed in the experimental structure as well in the optimized larger model is attributable to the aryl-aryl repulsive interactions between the terminal amido and the bridging imido groups. This repulsion is also reflected in the longer Sm-N_t bond for the larger model.

To gain a better understanding of the factors which favor asymmetric over symmetric bridging imido groups, an MO analysis of the simplified structure, presented in Figure 5(b), was undertaken. Figure 6 compares the results of the lower energy asymmetric structure (Figure 6a) with the symmetric structure (Figure 6b), where where the molecule was constrained in C_s symmetry. The two highest occupied MOs in this model are the same Sm-N $p\pi_{\perp}$ orbitals discussed previously in the full model (see Figure 4, MOs 147 and 148). The next highest MOs are the Sm-N $p\pi_{\parallel}$ orbitals, as in the previous picture, while the MOs involving the terminal NHPh ligand, which has been simplified to NH_2, are not present. It is instructive to compare the changes in orbital energies of the highest MOs in Figure 6 for the two different structures, although a rigorous correspondence with the total energy of the molecule in DFT calculations is problematic. One sees that the HOMO shows only a slight change. The next occupied orbital is

substantially lower in energy in the asymmetric structure, where it not only maintains a strong Sm_a=NPh bond interaction but also shows bonding interactions with Sm_b. Similarly a much lower orbital (bottom of Fig. 6) involving the C pπ orbitals of the phenyl ring shows some C_{ipso}-Sm_b bonding character. Thus, it appears that when N-Ph groups are employed, an asymmetric structure is favored due to (a) the overlap of the Npπ$_\perp$ orbital with the Sm_a 5d orbital and (b) the additional stabilization afforded by the formation of a weak C_{ipso}-Sm_b bond. In the case of imido groups such as N-$SiMe_3$, these interactions are not possible and a symmetric structure is observed.

Conclusions

Reaction of the π-arene bridged anilido dimer $[Sm(NHAr)_3]_2$ (**1**) (Ar = 2,6-*i*-$Pr_2C_6H_3$) with 4 equivalents of $AlMe_3$ leads to the formation of the bis-μ_2-imido complex $[(\mu\text{-ArN})Sm(\mu\text{-NHAr})(\mu\text{-Me})AlMe_2]_2$ (**2**). To the best of our knowledge this represents the first example of a structurally characterized 4f-element complex containing a discrete imido functionality. Although the isolation of compound **2** appears to be somewhat problematic, the structural elucidation of this molecule clearly demonstrates that the synthesis of species containing lanthanide main-group multiple bonds is feasible. DFT calculations indicate that the metal (acceptor) 5d orbitals play a significant role in stabilizing π-donation from the imido groups within the Sm_2N_2 core. We are currently developing new approaches toward the isolation of further novel examples of 4f-element complexes containing Ln=X multiple bonds (X = CR_2, NR, O). We envisage that these systems will not only provide us with new and interesting issues in structure and bonding, but may also provide some potentially reactive synthons with which to carry out a variety of small molecule transformations.

Experimental Section

General Considerations. All manipulations were carried out under an inert atmosphere of oxygen-free UHP grade argon using standard Schlenk techniques or under oxygen-free helium in a Vacuum Atmospheres glovebox. $AlMe_3$ (2.0 M hexane solution) was purchased from Aldrich and used as received. 2,6-di-*iso*-propylaniline was purchased from Aldrich, dried over molecular sieves and distilled prior to use. $Sm[N(SiMe_3)_2]_3$ was prepared according to a literature procedure.[56] Hexane and toluene were de-oxygenated by passage through a column of supported copper redox catalyst (Cu-0226 S) and dried by passing through a second column of activated

alumina. Hexamethyldisiloxane was distilled over sodium benzophenone and degassed prior to use. C_6D_6 was degassed, dried over Na-K alloy, and trap-to-trap distilled before use. ^1H NMR spectra were recorded on a Bruker AMX 500 spectrometer at ambient temperature. Infrared spectra were recorded on a Nicolet Avatar 360 FT-IR spectrometer as Nujol mulls between KBr plates. Elemental analyses were performed on a Perkin-Elmer 2400 CHN analyzer. Elemental analysis samples were prepared and sealed in tin capsules in the glovebox prior to combustion.

[Sm(μ-NHC$_6$H$_3$^{i}Pr$_2$-2,6)(NHC$_6$H$_3$^{i}Pr$_2$-2,6)$_2$]$_2$ (1). 2,6-di-*iso*-propylaniline (2.00 g, 11.0 mmol) in 10 mL toluene was added to a pale yellow toluene solution (50 mL) of Sm[N(SiMe$_3$)$_2$]$_3$ (2.30 g, 3.70 mmol). This caused the solution to turn red-orange. The reaction mixture was stirred at room temperature for 15 minutes, and then heated to reflux for 30 minutes. Upon cooling, a brick-red solid precipitated. The solvent was then removed under vacuum and the solid washed with hexane to remove HN(SiMe$_3$)$_2$. Slow evaporation of a saturated hexane solution yielded dark orange plates of **1** (1.30 g, 52% yield). The paramagnetism and low solubility of **1** in non-coordinating solvents did not allow for characterization by ^1H or $^{13}C\{^1H\}$ NMR spectroscopy. IR (Nujol, cm^{-1}): 1590 (m), 1575 (m), 1423 (s), 1358 (m), 1340 (m), 1324 (m), 1300 (m), 1250 (s), 1215 (m), 1193 (w), 1148 (w), 1138 (w), 1105 (m), 881 (m), 838 (m), 802 (s), 767 (s), 746 (s). Anal. Calcd. for $C_{72}H_{108}N_6Sm_2$: C, 63.66; H, 8.01; N, 6.19. Found: C, 63.02; H, 8.25; N, 5.94.

[(μ-NC$_6$H$_3$^{i}Pr$_2$-2,6)Sm(μ-NHC$_6$H$_3$^{i}Pr$_2$-2,6)(μ-Me)AlMe$_2$]$_2$ (2). 0.60 mL of a 2.0 M solution of AlMe$_3$ in hexane (1.20 mmol) was added to an orange slurry of **1** (400 mg, 0.300 mmol) in toluene (50 mL). Within a few minutes the slurry dissolved and the solution became deep red.

The solvent was removed under vacuum to produce a dark brown tacky solid. Hexane (10 mL) was added and the mixture pumped dry, again yielding a tacky solid. This procedure was then repeated. Following this, hexanes (20 mL) was added, the mixture filtered through a Celite pad, and the resulting filtrate concentrated to approximately 10 mL. This filtrate was then allowed to slowly evaporate under the glovebox atmosphere. Once at dryness, an oily orange-red solid resulted. This was washed with a minimal amount of cold hexanes (-10 °C) and pumped to dryness (yield 0.170 g). A 0.100 g sample of this solid was redissolved in hexanes (5 mL) and filtered through a Celite pad, and the resulting orange solution was allowed to slowly evaporate under the glovebox atmosphere. Once at dryness, an orange-red waxy crystalline solid resulted. A single-crystal X-ray diffraction study was carried out on a portion of this material, after which further vacuum was pulled on the solid to ensure complete dryness (yield 0.050 g). Anal. Calcd. for $C_{54}H_{88}Al_2N_4Sm_2$: C, 56.49; H, 7.73; N, 4.88. Found: C, 57.26; H, 8.32; N, 4.90.

Crystallographic Studies. Crystals of **1** and **2** were attached to a glass fiber using a spot of silicone grease. The crystals were mounted from a matrix of mineral oil under argon flow. The crystals were immediately placed on a Bruker P4/CCD/PC diffractometer, and cooled to 203 K using a Bruker LT-2 temperature device. The data were collected using a sealed, graphite monochromatized MoKα X-ray source. A hemisphere of data was collected using a combination of φ and ω scans, with 30 second frame exposures and 0.3º frame widths. Data collection and initial indexing and cell refinement was handled using SMART[58] software. Frame integration and final cell parameter calculations were carried out using SAINT[59] software. The final cell parameters were determined using a least-squares fit to 4402 reflections for **1**. The data

were corrected for absorption using the SADABS[60] program. Decay of reflection intensity was not observed.

The structures were solved in the space groups $P2_1/n$ for **1** and $C2/c$ for **2** using Direct methods and difference Fourier techniques. The initial solutions revealed the samarium and the majority of all non-hydrogen atom positions. The remaining atomic positions were determined from subsequent Fourier synthesis. The amide hydrogen atom positions were found on the difference maps, and refined with the isotropic temperature factor set to 0.08 $Å^2$. All other hydrogen atom positions were idealized (C-H = 0.98 Å for methine, 0.97 Å for methylene, 0.96 Å for methyl, and 0.93 Å for aromatic). The idealized hydrogen atoms were refined using the riding model, with isotropic temperature factors fixed to 1.2 times the equivalent isotropic U of the carbon atom they were bound to. The final refinement[61] included anisotropic temperature factors on all non-hydrogen atoms. Structure solution, refinement, graphics, and preparation of publication materials were performed using SHELXTL NT.[62] Additional details of data collection and structure refinement are listed in Table 3.

Details of Theoretical Calculations. All calculations were carried out using the B3LYP functional[63,64] by using a "large core" effective potential[65;66] on the samarium atom including shells up to the filled 4s, 4p and 4d shells in the core. In addition, the partially filled $4f^5$ shell, corresponding to the configuration of Sm(III), was also included in the core for a total of 51 electrons. The remaining 11 electrons were treated explicitly which includes the "outer core" $5s^2$ $5p^6$ electrons and the valence $6s^2$ $5d^1$ electrons. A valence [5s, 4p, 3d] basis set was employed. 6-31G basis sets were used for C, N, Al and H atoms. All calculations were carried out with Gaussian 98.[67]

Acknowledgments

We acknowledge support from Laboratory Directed Research and Development at Los Alamos and from the Office of Basic Energy Sciences, Division of Chemical Sciences, U.S. Department of Energy. Los Alamos National Laboratory is operated by the University of California for the U.S. Department of Energy under Contract W-7405-ENG-36.

Supporting Information Available

Listings of fractional atomic coordinates, bond lengths and angles, anisotropic thermal parameters and hydrogen atom coordinates for complexes **1** and **2**, and coordinates of the optimized model structure $[(\mu\text{-PhN})Sm(\mu\text{-NHPh})(\mu\text{-Me})AlMe_2]_2$ from DFT calculations (xx pages). This material is available free of charge via the Internet at http://pubs.acs.org.

References

(1) Los Alamos National Laboratory: a) C-SIC, Mail Stop J514, b) NMT-DO, Mail Stop J514, c) G. T. Seaborg Institute, Mail Stop E500, d) T-12, Mail Stop B268, e) C-SIC, Mail Stop G739.

(2) Universitè de Bourgogne.

(3) Mountford, P. *Chem. Commun.* **1997**, 2127.

(4) Danopoulos, A. A.; Green, J. C.; Hursthouse, M. B. *J. Organomet. Chem.* **1999**, *591*, 36.

(5) Schrock, R. R. *Tetrahedron* **1999**, *55*, 8141.

(6) Romao, C. C.; Kuehn, F. E.; Herrmann, W. A. *Chem. Rev.* **1997**, *97*, 3197.

(7) Che, C. M. *Pure Appl. Chem.* **1995**, *67*, 225.

(8) Wigley, D. E. *Prog. Inorg. Chem.* **1994**, *42*, 239.

(9) Nugent, W. A.; Mayer, J. M. *Metal-Ligand Multiple Bonds*; Wiley-Interscience: New York, 1988.

(10) Zuckerman, R. L.; Krska, S. W.; Bergman, R. G. *J. Am. Chem. Soc.* **2000**, *122*, 751.

(11) Wang, W. D.; Espenson, J. H. *Organometallics* **1999**, *18*, 5170.

(12) Birdwhistell, K. R.; Lanza, J.; Pasos, J. *J. Organomet. Chem.* **1999**, *584*, 200.

(13) Polse, J. L.; Andersen, R. A.; Bergman, R. G. *J. Am. Chem. Soc.* **1998**, *120*, 13405.

(14) Lee, S. Y.; Bergman, R. G. *Tetrahedron* **1995**, *51*, 4255.

(15) McGrane, P. L.; Jensen, M.; Livinghouse, T. *J. Am. Chem. Soc.* **1992**, *114*, 5459.

(16) Blake, R. E.; Antonelli, D. M.; Henling, L. M.; Schaefer, W. P.; Hardcastle, K. I.; Bercaw, J. E. *Organometallics* **1998**, *17*, 718.

(17) Walsh, P. J.; Hollander, F. J.; Bergman, R. G. *J. Am. Chem. Soc.* **1988**, *110*, 8729.

(18) Brennan, J. G.; Andersen, R. A. *J. Am. Chem. Soc.* **1985**, *107*, 514.

(19) Burns, C. J.; Smith, W. H.; Huffman, J. C.; Sattleberger, A. P. *J. Am. Chem. Soc.* **1990**, *112*, 3237.

(20) Arney, D. S. J.; Bruck, M. A.; Huber, S. R.; Wigley, D. E. *Inorg. Chem.* **1992**, *31*, 3749.

(21) Brown, D. R.; Denning, R. G.; Jones, R. H. *Chem. Commun.* **1994**, 2601.

(22) Stewart, J. L.; Andersen, R. A. *New J. Chem.* **1995**, *19*, 587.

(23) Straub, T.; Frank, W.; Reiss, G. J.; Eisen, M. S. *Dalton Trans.* **1996**, 2541.

(24) Peters, R. G.; Warner, B. P.; Burns, C. J. *J. Am. Chem. Soc.* **1999**, *121*, 5585.

(25) Diaconescu, P. L.; Arnold, P. L.; Baker, T. A.; Mindiola, D. J.; Cummins, C. C. *J. Am. Chem. Soc.* **2000**, *122*, 6108.

(26) Trifonov, A. A.; Bochkarev, M. N.; Schumann, H.; Loebel, J. *Angew. Chem., Int. Ed. Engl.* **1991**, *30*, 1149.

(27) Xie, Z.; Wang, S.; Yang, Q.; Mak, T. C. W. *Organometallics* **1999**, *18*, 1578.

(28) Evans, W. J.; Ansari, M. A.; Ziller, J. W.; Khan, S. I. *Inorg. Chem.* **1996**, *35*, 5435.

(29) After submission of this paper, the synthesis and characterization of two related ytterbium imido complexes were reported. See: Chan, H.-S.; Li, H.-W.; Xie, Z. *Chem. Commun.* **2002**, 652.

(30) Bradley, D. C.; Ghotra, J. S.; Hart, F. A. *Dalton Trans.* **1973**, 1021.

(31) Barnhart, D. M.; Clark, D. L.; Gordon, J. C.; Huffman, J. C.; Vincent, R. L.; Watkin, J. G.; Zwick, B. D. *Inorg. Chem.* **1994**, *33*, 3487.

(32) Cotton, F. A.; Schwotzer, W. *J. Am. Chem. Soc.* **1986**, *108*, 4657.

(33) Fan, B. C.; Shen, Q.; Lin, Y. H. *J. Organomet. Chem.* **1989**, *377*, 51.

(34) Deacon, G. B.; Nickel, S.; MacKinnon, P.; Tiekink, E. R. T. *Aust. J. Chem.* **1990**, *43*, 1245.

(35) Brennan, J. G.; Cloke, F. G. N.; Sameh, A. A.; Zalkin, A. J. *Chem. Commun.* **1987**, 1668.

(36) Fryzuk, M. D.; Love, J. B.; Rettig, S. J. *J. Am. Chem. Soc.* **1997**, *119*, 9071.

(37) Fryzuk, M. D.; Jafarpour, L.; Kerton, F. M.; Love, J. B.; Patrick, B. O.; Rettig, S. J. *Organometallics* **2001**, *20*, 1387.

(38) Minhas, R. K.; Ma, Y.; Song, J. I.; Gambarotta, S. *Inorg. Chem.* **1996**, *35*, 1866.

(39) Evans, W. J.; Olofson, J. M.; Ziller, J. W. *Inorg. Chem.* **1989**, *28*, 4308.

(40) We have also synthesized and characterized the lanthanum derivative, $[La(NHAr)_3]_2$; X-ray crystallography shows the same π-arene bridged structure in the solid state. ^1H and $^{13}C\{^1H\}$

NMR spectroscopy are consistent with a dimeric structure being maintained in solution. Giesbrecht, G. R., Gordon, J. C., Clark, D. L., Scott, B. L., unpublished results.

(41) Giesbrecht, G. R.; Gordon, J. C.; Brady, J. T.; Clark, D. L.; Keogh, D. W.; Michalczyk, R.; Scott, B. L.; Watkin, J. G. *Eur. J. Inorg. Chem.* **2002**, in press.

(42) Attempts to prepare the lanthanum analog $[(\mu\text{-ArN})La(\mu\text{-NHAr})(\mu\text{-Me})AlMe_2]_2$ by the reaction of $[La(NHAr)_3]_2$ with trimethylaluminum were not successful.

(43) Brady, E. D., Keogh, D. W., Scott, B. L., Watkin, J. G., unpublished results.

(44) Evans, W. J.; Kociok-Kohn, G.; Leong, V. S.; Ziller, J. W. *Inorg. Chem.* **1992**, *31*, 3592.

(45) Brennan, J. G.; Andersen, R. A.; Zalkin, A. *J. Am. Chem. Soc.* **1988**, *110*, 4554.

(46) Schnabel, R. C.; Scott, B. L.; Smith, W. H.; Burns, C. J. *J. Organomet. Chem.* **1999**, *591*, 14.

(47) Wirringa, U.; Roesky, H. W.; Noltemeyer, M.; Schmidt, H. G. *Inorg. Chem.* **1994**, *33*, 4607.

(48) Gordon, J. C.; Giesbrecht, G. R.; Brady, J. T.; Clark, D. L.; Keogh, D. W.; Scott, B. L.; Watkin, J. G. *Organometallics* **2002**, in press.

(49) Evans, W. J.; Chamberlain, L. R.; Ulibarri, T. A.; Ziller, J. W. *J. Am. Chem. Soc.* **1988**, *110*, 6423.

(50) Evans, W. J.; Boyle, T. J.; Ziller, J. W. *J. Am. Chem. Soc.* **1993**, *115*, 5084.

(51) Evans, W. J.; Boyle, T. J.; Ziller, J. W. *J. Organomet. Chem.* **1993**, *462*, 141.

(52) Biagini, P.; Lugli, G.; Abis, L.; Millini, R. *J. Organomet. Chem.* **1994**, C16.

(53) Maron, L.; Eisenstein, O. *J. Phys. Chem. A* **2000**, *104*, 7140.

(54) Maron, L.; Eisenstein, O. *New J. Chem.* **2001**, *25*, 255.

(55) Clark, D. L., Gordon, J. C., Hay, P. J., Poli, R, unpublished results.

(56) Brady, E. D., Clark, D. L., Gordon, J. C., Hay, P. J., Keogh, D. W., Martin, R. L., Poli, R., unpublished results.

(57) Evans, W. J.; Golden, R. E.; Ziller, J. W. *Inorg. Chem.* **1991**, *30*, 4963.

(58) *SMART* Version 4.210; Bruker Analytical X-ray Systems, Inc.: Madison, WI 53719, 1996.

(59) *SAINT* Version 4.05; Bruker Analytical X-ray Systems, Inc.: Madison, WI 53719, 1996.

(60) Sheldrick, G. *SADABS*, first release; University of Gottingen: Germany.

(61) $R_1 = \Sigma||F_o| - |F_c||/\Sigma|F_o|$ and $R_{2w} = [\Sigma[w(F_o^2 - F_c^2)^2]/\Sigma[\omega(F_o^2)^2]]^{1/2}$; $w = 1/[\sigma^2(F_o^2) + (aP)^2]$, where a = 0.0393(2), 0.0285(3), and 0.0719(4).

(62) *SHELXTL* NT Version 5.10; Bruker Analytical X-ray Instruments, Inc.: Madison, WI 53719, 1997.

(63) Becke, A. D. *J. Chem. Phys.* **1993**, *98*, 5648.

(64) Lee, C. T.; Yang, W. T.; Parr, R. G. *Phys. Rev. B* **1988**, *37*, 785.

(65) Dolg, M.; Stoll, H.; Savin, A.; Preuss, H. *Theor. Chim. Acta* **1989**, *75*, 173.

(66) Dolg, M.; Stoll, H.; Preuss, H. *Theor. Chim. Acta* **1993**, *85*, 441.

(67) Frisch, M. J.; Trucks, G. W.; Schlegel, H. B.; Scuseria, G. E.; Robb, M. A.; Cheeseman, J. R.; Zakrzewski, V. G.; Montgomery, J. A., Jr.; Stratmann, R. E.; Burant, J. C.; Dapprich, S.; Millam, J. M.; Daniels, A. D.; Kudin, K. N.; Strain, M. C.; Farkas, O.; Tomasi, J.; Barone, V.; Cossi, M.; Cammi, R.; Mennucci, B.; Pomelli, C.; Adamo, C.; Clifford, S.; Ochterski, J.; Petersson, G. A.; Ayala, P. Y.; Cui, Q.; Morokuma, K.; Malick, D. K.; Rabuck, A. D.; Raghavachari, K.; Foresman, J. B.; Cioslowski, J.; Ortiz, J. V.; Stefanov, B. B.; Liu, G.; Liashenko, A.; Piskorz, P.; Komaromi, I.; Gomperts, R.; Martin, R. L.; Fox, D. J.; Keith, T.; Al-

Laham, M. A.; Peng, C. Y.; Nanayakkara, A.; Gonzalez, C.; Challacombe, M.; Gill, P. M. W.; Johnson, B. G.; Chen, W.; Wong, M. W.; Andres, J. L.; Head-Gordon, M.; Replogle, E. S.; Pople, J. A. Gaussian 98, revision A.9; Gaussian, Inc.: Pittsburgh, PA 1998.

Table 1. Selected Bond Distances (Å) and Angles (deg) for [Sm(μ-NHC$_6$H$_3$^{i}Pr$_2$-2,6)(NHC$_6$H$_3$^{i}Pr$_2$-2,6)$_2$]$_2$ (1)

Sm1-N1	2.241(8)	Sm1-N2	2.351(10)
Sm1-N3	2.273(11)	Sm1-arene(cent)	2.596
Sm1-C13	3.094(10)	Sm1-C14	3.018(10)
Sm1-C15	2.870(10)	Sm1-C16	2.838(10)
Sm1-C17	2.881(10)	Sm1-C18	3.013(9)
N1-Sm1-N2	92.6(3)	N1-Sm1-N3	112.5(4)
N1-Sm1-arene(cent)	109.5	N2-Sm1-N3	117.3(3)
N2-Sm1-arene(cent)	104.3	N3-Sm1-arene(cent)	117.6

Table 2. Selected Bond Distances (Å) and Angles (deg) for [(μ-NC$_6$H$_3$^{i}Pr$_2$-2,6)Sm(μ-NHC$_6$H$_3$^{i}Pr$_2$-2,6)(μ-Me)AlMe$_2$]$_2$ (2)

Sm1-N1	2.271(7)	Sm1-N1*	2.152(8)
Sm1-N2	2.535(8)	Sm1-C1	2.666(8)
Sm1-C25	2.649(14)	N1-C1	1.387(12)
Al1-C25	2.094(12)	Al1-C26	1.939(12)
Al1-C27	1.971(11)	N1-Sm1-N1*	81.1(3)
N1-Sm1-N2	127.1(3)	N1-Sm1-C1	31.3(3)
N1-Sm1-C25	110.8(4)	N1*-Sm1-N2	151.6(3)
N1*-Sm1-C1	112.0(3)	N1*-Sm1-C25	99.6(4)
N2-Sm1-C1	95.8(3)	N2-Sm1-C25	75.4(3)
C1-Sm1-C25	109.1(4)		

Table 3. Crystallographic Data

Compound	**1**	**2**
Formula	$C_{72}H_{108}N_6Sm_2$	$C_{54}H_{88}Al_2N_4Sm$
Molecular Weight	1358.34	1105.91
Temperature, K	203(2)	203(2)
Crystal System	monoclinic	monoclinic
Space Group	$P2_1/n$	$C2/c$
Crystal Size, mm	0.21 x 0.21 x 0.21	0.06 x 0.12 x 0.12
a, Å	19.363(2)	15.912(1)
b, Å	9.4027(9)	18.635(1)
c, Å	20.063(2)	18.941(1)
α, °	90	90
β, °	110.193(2)	90.709(2)
γ, °	90	90
V, Å^3	3428.3(6)	5616.0(7)
Z	2	4
D_{calc}, g/mL	1.316	1.308
Absorption coeffiecient, mm^{-1}	1.739	2.133
F(000)	1412	2276
Theta range, °	1.26 to 23.33	1.7 to 23.4
Total reflections	10114	7377
Independent reflections	4711	3709

GOF	1.047	1.366
R1	0.0704	0.0581
wR2	0.0917	0.1396

Table 4. Comparison of calculated and experimental structural parameters for [(μ-ArN)Sm(μ-NHAr)(μ-Me)AlMe$_2$]$_2$ (Ar = 2,6-*i*-Pr$_2$C$_6$H$_3$) and related model compounds

		Bond lengths (Å)				
Ar substituent		Sm=N_{br}	Sm-N_{br}	Diff.	Sm-N_t	<Sm-N_{br}-R (°)
[(μ-ArN)Sm(μ-NHAr)(μ-Me)AlMe$_2$]$_2$ species:						
2,6-*i*-Pr$_2$C$_6$H$_3$	Exptl.	2.153	2.271	0.118	2.535	168
Ph	Calc.	2.220	2.299	0.079	2.549	153
Ph (no AlMe$_3$)	Calc.	2.206	2.319	0.113	2.318	157
Ph (no Sm 5d)	Calc.	2.308	2.425	0.117	2.544	160
[(μ-MeN)Sm(μ-NHMe)(μ-Me)AlMe$_2$]$_2$ species:						
Me	Calc.	2.247	2.253	0.006	2.458	131
[(μ-PhN$_{br}$)Sm(μ-NH$_2$)(μ-Me)AlH$_2$]$_2$ species:						
Ph	Calc.	2.183	2.346	0.163	2.440	161

Table 5. Analysis of selected orbitals for [(μ-PhN)Sm(μ-NHPh)(μ-Me)AlMe$_2$]$_2$

MO	ε(a.u.)	Description	%s,p Sm_a	%d Sm_a	%s,p Sm_b	%d Sm_b	%total ligand
149	-0.049	Sm 6s, 5d (LUMO)	20.0	26.0	21.0	25.0	8.0
148	-0.189	Sm-N_{br} $\pi_{\perp}$(HOMO)	1.0	3.3	1.0	3.2	91.5
147	-0.206	Sm-N_{br} $\pi_{\perp}$	0.6	7.5	0.8	7.6	83.5
146	-0.215	Sm-N_{br} $\pi_{\parallel}$	0.3	6.7	0.3	6.5	86.2
145	-0.220	Sm-N_t $\pi_{\perp}$	0.8	2.3	0.7	2.4	93.8
144	-0.225	Sm-N_t $\pi_{\perp}$	0.3	2.8	0.3	2.8	93.8
143	-0.234	Sm-N_{br} $\pi_{\parallel}$	1.9	6.1	1.9	6.1	84.0

Scheme 1

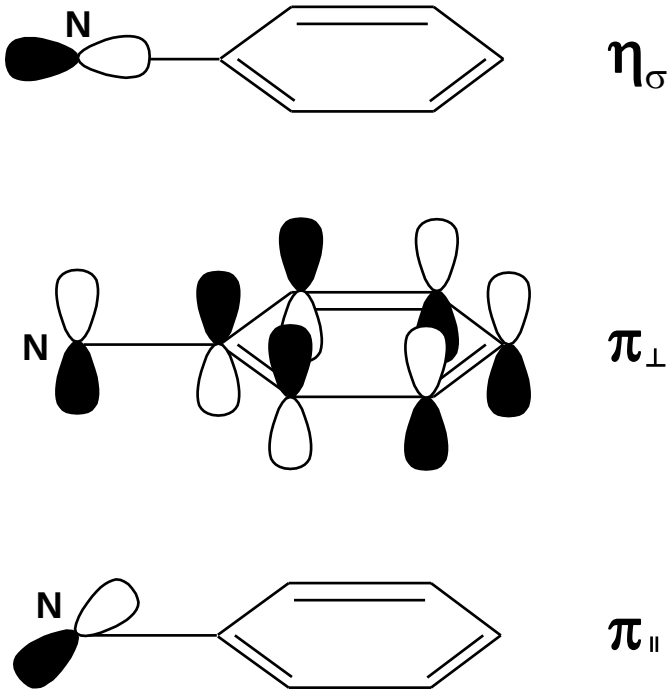

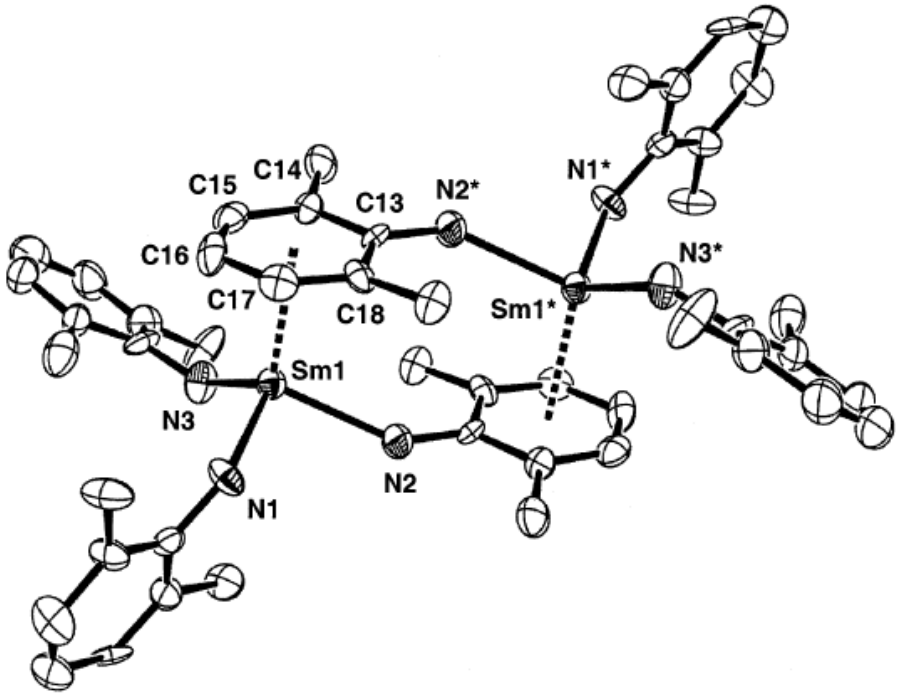

Figure 1. ORTEP view of [Sm(μ-$NHC_6H_3{}^iPr_2$-2,6)($NHC_6H_3{}^iPr_2$-2,6)$_2$]$_2$ (**1**) drawn with 30% probability ellipsoids. Isopropyl methyl groups have been omitted for clarity.

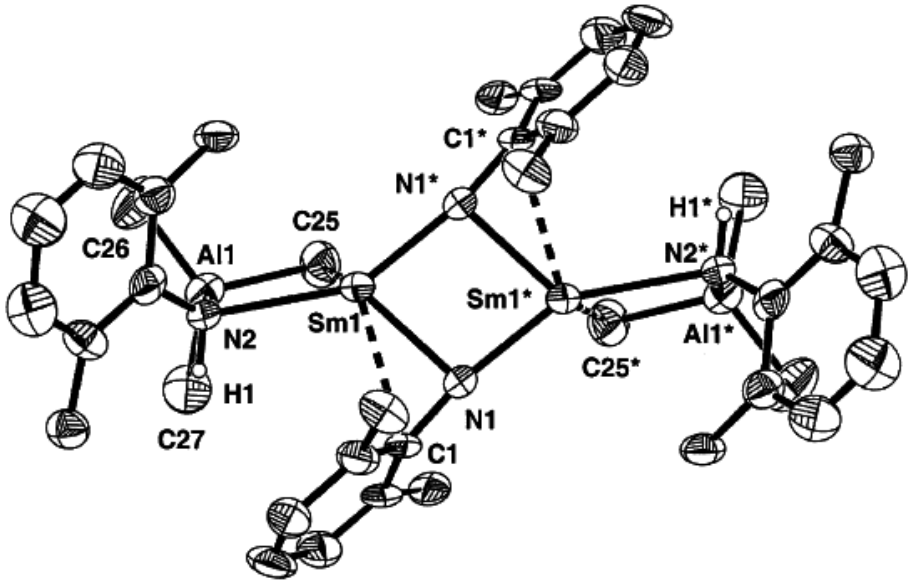

Figure 2. ORTEP view of [(μ-$NC_6H_3{}^iPr_2$-2,6)Sm(μ-$NHC_6H_3{}^iPr_2$-2,6)(μ-Me)$AlMe_2$]$_2$ (**2**) drawn with 30% probability ellipsoids. Isopropyl methyl groups have been omitted for clarity.

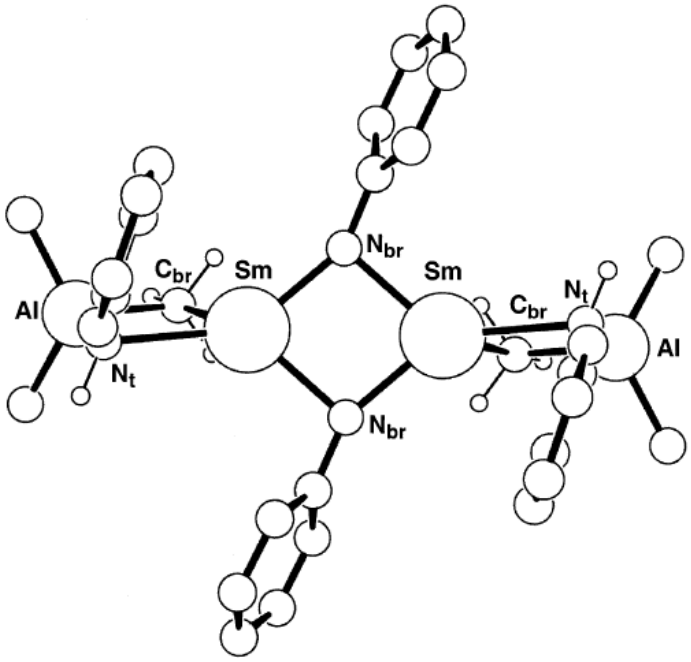

Figure 3. View of the fully optimized $[(\mu\text{-PhN})Sm(\mu\text{-NHPh})(\mu\text{-Me})AlMe_2]_2$ structure from B3LYP calculations.

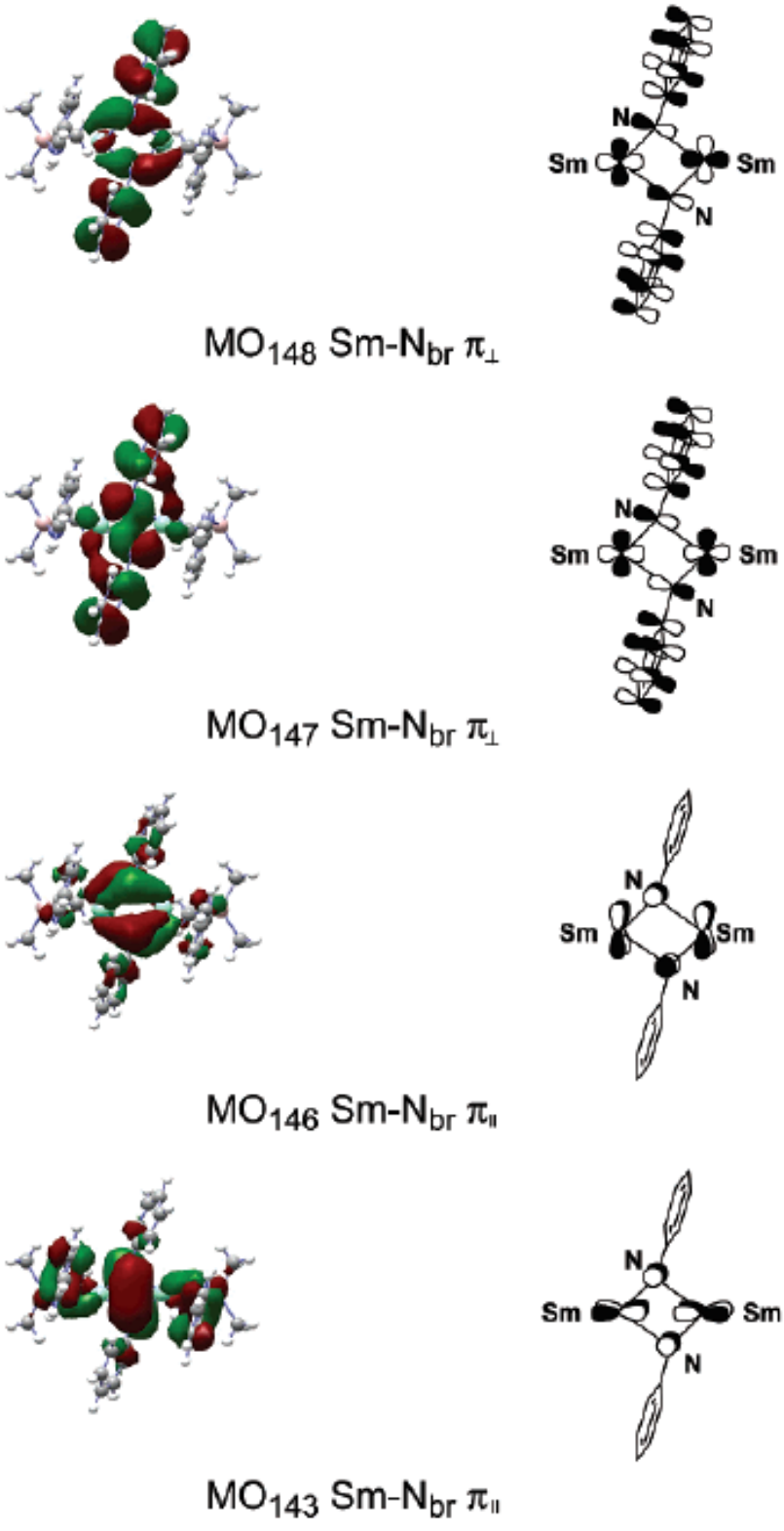

Figure 4. Contour plots (left) and ChemDraw representations (right) of the highest occupied molecular orbitals for the $[(\mu\text{-PhN})Sm(\mu\text{-NHPh})(\mu\text{-Me})AlMe_2]_2$ model from DFT calculations.

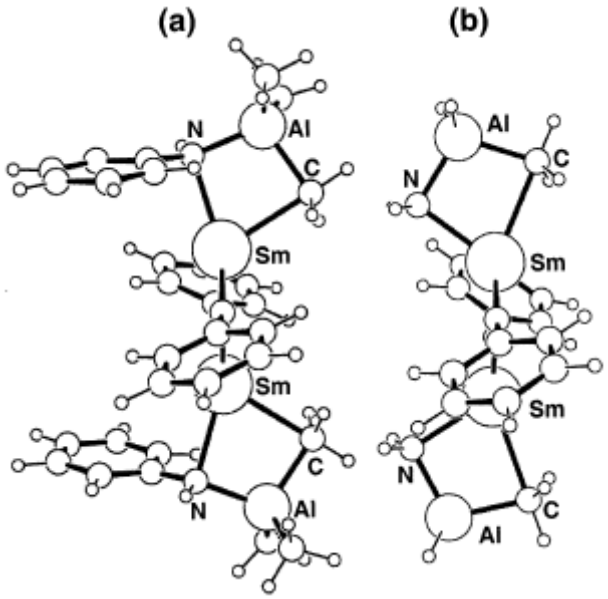

Figure 5. Views of the fully optimized $[(\mu\text{-PhN})Sm(\mu\text{-NHR})(\mu\text{-Me})AlR'_2]_2$ models.

(a) R = Ph, R' = Me; (b) R = R' = H.

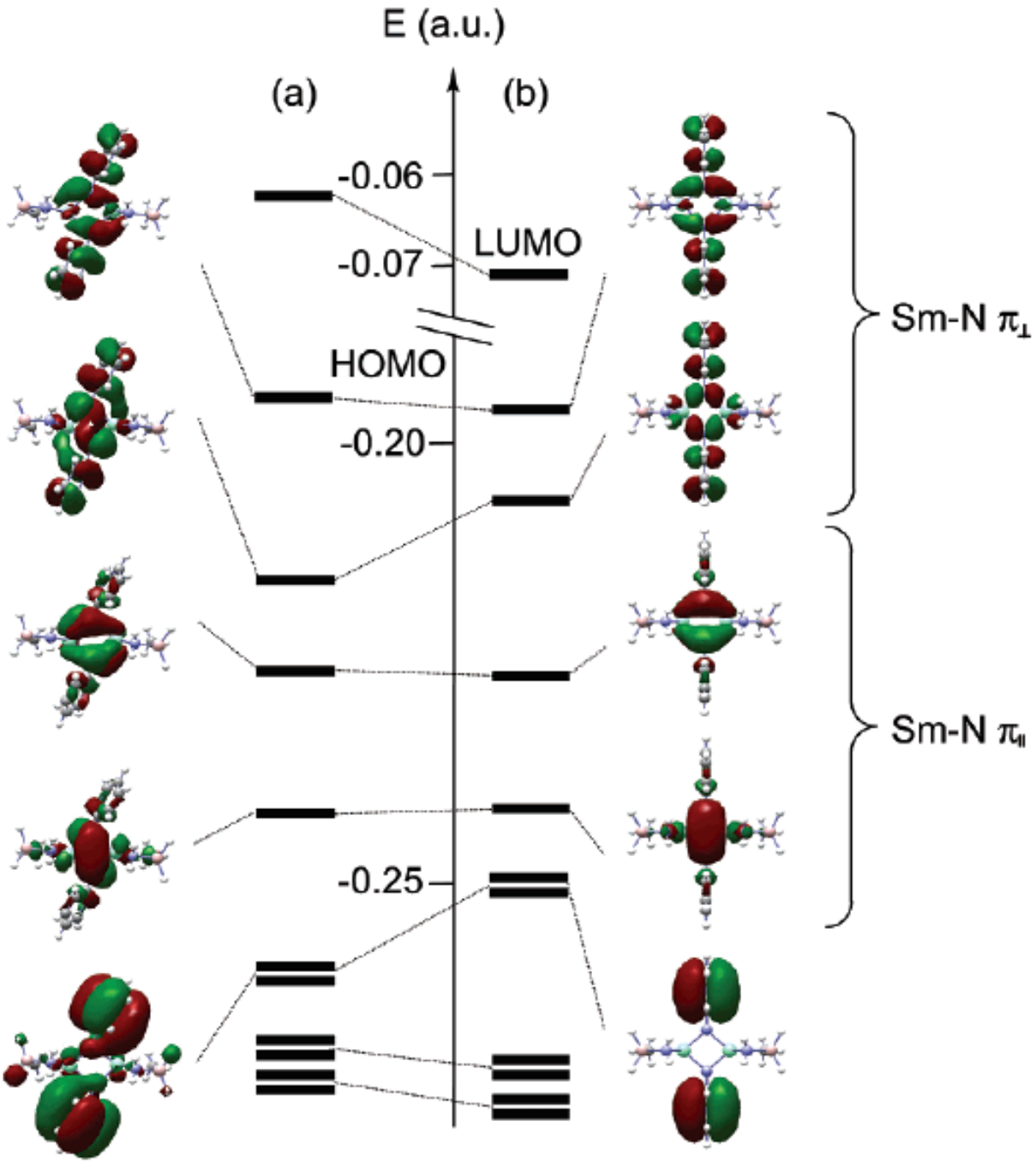

Figure 6. MO diagram and contour plots of selected orbitals for the model compound $[(\mu\text{-PhN})Sm(\mu\text{-}NH_2)(\mu\text{-Me})AlH_2]_2$. (a) optimized tilted geometry; (b) partially optimized geometry in C_{2v} symmetry.